J Wood Sci (2006) 52:411–421
DOI 10.1007/s10086-005-0802-z

ORIGINAL ARTICLE

Masahiro Noguchi · Kohei Komatsu

Estimation of stiffness and strength in timber knee joints with adhesive and verification by experiment

Received: October 22, 2004 / Accepted: November 18, 2005 / Published online: June 29, 2006

Abstract The use of adhesive joints is gradually increasing, especially those with glued-in steel rods (GIRs). There are, however, some problems with the design methods when used for moment-transmitting applications. In this article, design methods for GIRs and cross-lapped glued joints (CLJs) are proposed. For CLJs, we made a hypothesis that both rotational deformation of CLJ and stress of the glue line occurred with bending and shearing deformation of the timber. Using this hypothesis and Kelvin's theorem, a mechanical model of CLJ is proposed. For GIRs, the axial stress component of the rod and the lateral stress component of the rod were taken into account using the theory of a beam on an elastic foundation. From the comparisons between calculations and experimental results, it was recognized that the stiffness and strength of CLJs and GIRs could be predicted precisely using our proposed models.

Key words Glued-in rod · Knee joint · Timber · Cross-lapped joint · Mechanical model

Introduction

The use of adhesive joints is gradually increasing, especially those with glued-in steel rods (GIRs). However, there are some problems with the design methods when used for moment-transmitting applications. No model for cross-lapped joints (CLJs) can adequately explain why the rotational rigidity of CLJs is not infinite, although some mechanical models[1–4] have considered the stress distribution of the glue line. In addition, from the design viewpoint, there are no design methods describing the rotational stiffness. The reason is that the previous models were derived based on a hypothesis that a moment-resisting joint must rotate at the starting points. Thus, it is necessary to build a mechanical model explaining how rotation occurs in CLJs and to develop a design equation.

Previous models of GIRs[5] take into account only the axial component of the rods. In fact, two resisting components of rods exist, i.e., lateral and axial. There are two disadvantages in the previous models. The first is the stiffness of a moment-resisting joint with GIRs. Previous models were rooted from the simulation of a panel zone in a reinforced concrete structure. However, it is well known that timber cannot be assumed to be a rigid body, especially for a dowel-type shear joint like rods. Therefore, the lateral component must be incorporated. The second disadvantage is the strength of this type of joint. Not only does pulling failure occur with rods, but also splitting failures due to lateral force components. Because the lateral force components are ignored in previous models,[5] the splitting failure criterion caused by the lateral force components is not taken into account. The splitting failures result in brittle failure of a moment-resisting joint. Therefore, it is important to derive a mechanical model incorporating the splitting failure due to lateral force components caused by an applied bending moment.

The developed mechanical model should be able to explain why CLJs rotate and the developed design method for steel rods with glue should consider both axial and lateral force components. In this article, new design methods for GIR joints, and CLJs are proposed for transmitting bending moments.

M. Noguchi (✉)
Stractural Engineering Research Center, Tokyo Institute of Technology, R3-18, 4259 Nagatsuta, Midori-ku, Yokohama 226-8503, Japan
Tel. +81-45-924-5352; Fax +81-45-924-5364
e-mail: mnoguchi@serc.titech.ac.jp

K. Komatsu
Research Institute for Sustainable Humanosphere, Kyoto University, Uji 611-0011, Japan

Experimental

Five specimen types were prepared. Figures 1 and 2 show the specimens used in this study. Differences are associated with the number of members and the use of GIRs. In type

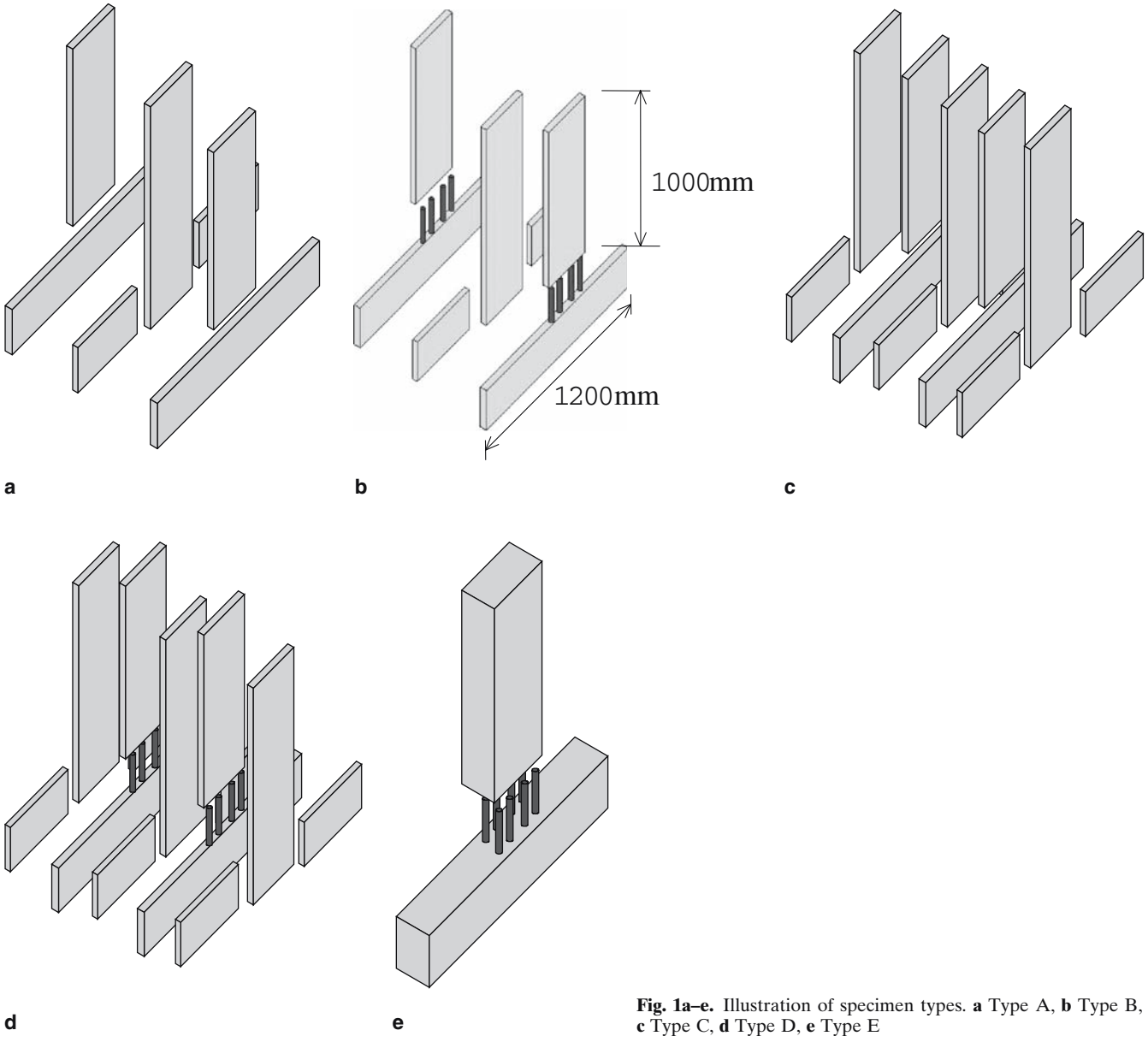

Fig. 1a–e. Illustration of specimen types. **a** Type A, **b** Type B, **c** Type C, **d** Type D, **e** Type E

A, in Fig. 1a, all the members consist of three layers (each layer width was 36 mm). Type B specimens were assembled in the same way, but two layers were connected using glued-in rod, as shown in Fig. 1b. Type C and D specimens were assembled with five layers (each layer width was 20 mm), as in Fig. 1c, d, where type D specimens had two layers with glued-in rod. Type E specimens were assembled traditionally with one layer, as shown in Fig. 1e. The dimensional cross sections of the three-layer specimens, the five-layer specimens, and single-layer specimens were 200 × 108 mm, 200 × 105 mm, and 200 × 120 mm (height × thickness), respectively. The other dimensions of the specimens are described in Fig. 3. Three specimens were set for each joint type except for type E, for which two specimens were set.

All specimens were glued-laminated using sugi having JAS (Japanese Agricultural Standard) strength grade of E65–f 225 [modulus of elasticity (MOE) 6500 MPa, modulus of rupture (MOR) 22 MPa, composition of lamina L80 L60 L50 L50 L50 L60 L80); the average moisture content was 11%. The glued-in steel rods were located as shown in Fig. 2. An epoxy resin adhesive (polyamidoamine epoxy resin = 1:1) was used to glue each layer and to fill any voids. All layers were glued. The inserted length of the steel rod (ss400, Japanese Industrial Standard) in each member was set to 100 mm. The rod diameter was 16 mm and the pre-drilled holes were 18 mm in diameter. The time to cure was at least 2 weeks under natural conditions (around 10°C). The tests were performed with a monotonic load using a hydraulic actuator until failure appeared and the load dropped drastically. The load was applied by a lateral force at the top of the specimens, as illustrated in Fig. 3.

The load speeds of the applied point were around 1 mm/s by manual control. The load at the applied point (P) was

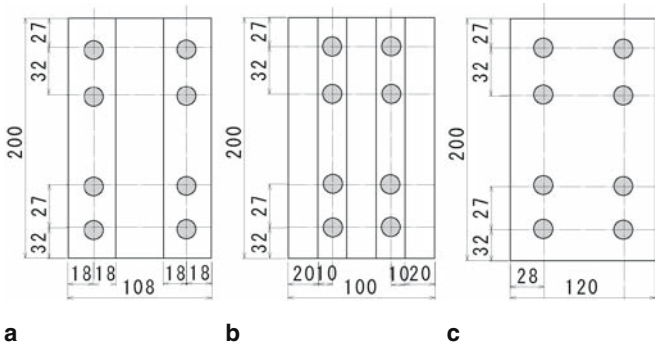

Fig. 2. Arrangement of rods for **a** type B, **b** type D, and **c** type E

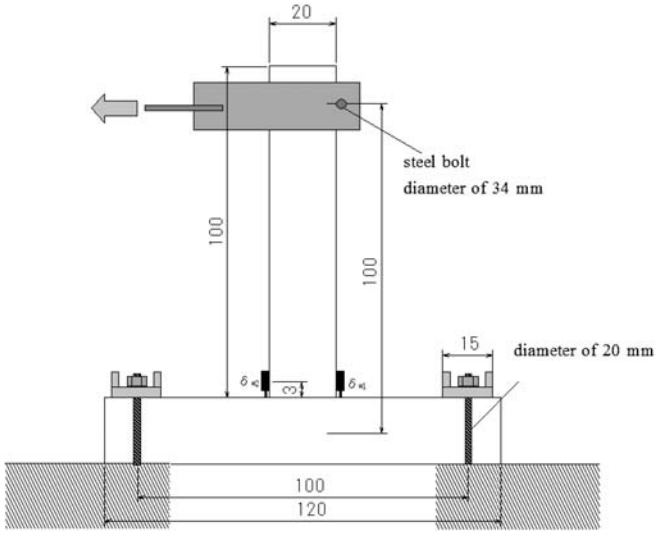

Fig. 3. Test setup

measured using a load cell. The moment worked in the joint (M) was defined as:

$$M = 1 \times P \tag{1}$$

The displacement gauges were located as shown in Fig. 3, and the rotational angle of BCLJ (θ) is defined as follows:

$$\theta = \frac{\delta_{\#1} - \delta_{\#2}}{240} \tag{2}$$

Results wand discussion

Strength

Figure 4 gives an overview of the bending capacity of all joint types. It should be noted that the strength of Type B joint exceeded the mean bending capacity of a solid beam of the same grade and cross section as the specimen. The strengths of the other joints varied from 70% to 90% of the mean bending capacity of a solid beam. The fact that the mean strength of type D was less than type C is because of

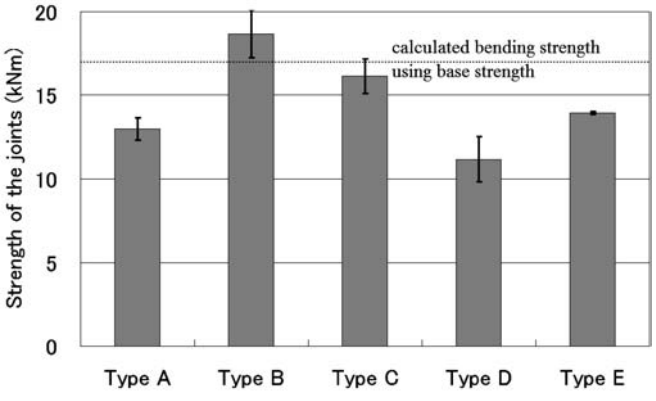

Fig. 4. Test results for the strength of the joints, given as mean bending strength. *Bars* show SD

splits that originated from the holes. Because of the drilled holes, the wood fibers are not continuous like in type C specimens and a weak spot is created. In this respect, the diameter of the hole might have been too large when compared with the width of the layers. In type B specimens, the bending failure of timber at the interface between beam and column and the pulling out of steel occurred simultaneously. In CLJ specimens (types A and C), bending failure of timber occurred at the interface between beam and column. In type E specimens, two different failure modes appeared. One specimen failed with splits occurring at the panel zone due to pulling out of the rod; another specimen failed by splitting failure caused by the lateral load component of the rods.

Stiffness

The analyses are presented based on the evaluation of the test data to assess the influences of certain parameters and their effects in relation to the rotational stiffness. The joints that combine both CLJs and GIRs were compared with type C (CLJ). Figure 5 gives an overview of the stiffness of all types of joints. If we compare the types with and without GIRs, Fig. 5 shows that the use of GIRs is beneficial for the rotational stiffness for the same number of layers.

Next, the effect of the number of glue lines was evaluated. The glued area for type A specimens is smaller than that for type C. While the dimensions of the members are almost the same for types A and C the number of layers and therefore the number of glue lines are different. Type C has five layers and four glue lines, while type A has three layers and two glue lines. The rotational stiffness appears to be almost proportional to the number of glue lines. From this, it is clear that the number of glue lines influences the rotational stiffness of the moment-resisting joints. The detail of this influence is discussed below.

The joints with both GIRs and CLJs were examined with types A, B, and E being the focus. The rotational stiffness of type B is smaller than that of type E, although type B is a CLJ and includes GIRs. From this observation, it follows that the rotational stiffness of CLJs with GIRs cannot

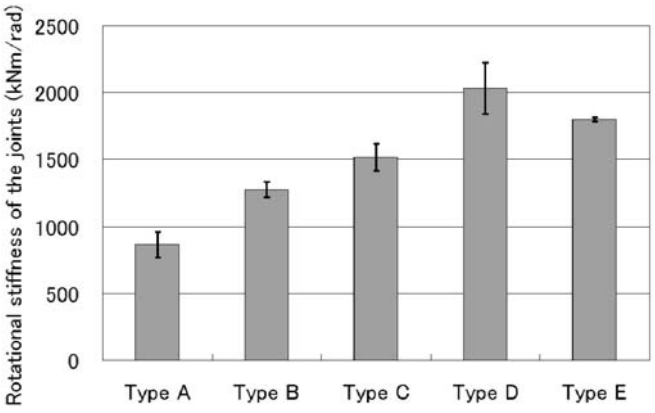

Fig. 5. Test results for the rotational stiffness of the joints. *Bars* show SD

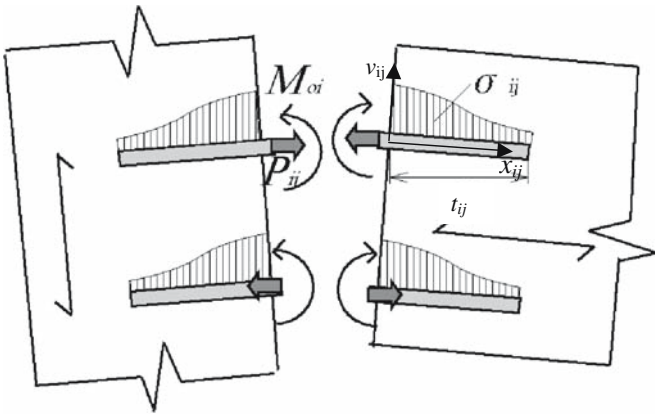

Fig. 6. Equilibrium at the interface. t_{ij}, embedment length of the rod in the column; v_{ijx}, bearing displacement of rod at x_{ij}; σ_{xij}, lateral stress; x_{ij}, distance from the interface between beam and column; M_{oi}, the bending moment of the *i*-th rod at the interface resulting from the lateral force component of the rods inserted in the beam; P_{ij}, the axial force of the *i*-th rods

simply be explained by a parallel spring model. If using a parallel spring concept, type B must be higher than type E.

Comparing the rotational stiffness results in Fig. 5 for type C (CLJ), type D (CLJ + GIR), and type E (GIR), it shows type C with the lowest and type D with the highest values. From this it can be concluded that the rotational stiffness of a moment-resisting joint that combines CLJ and GIRs cannot simply be explained as a series system of springs of CLJ and GIRs. If using the series spring concept, type E must be higher than type D. Quantitative analysis and evaluation of this effect is discussed below using a theoretical model.

Model for a moment-resisting joint with glued-in rods

Concept

In our model, each component was modeled as simply as possible, because the aim of this model was to make it suitable as a practical design method. When the joint rotates, the lateral deformations of rods must occur as well as the axial deformations of rods, considering the compatibility of the joint. In the model below, two resisting components of the joints were taken into account. The first is the resisting-moment component of the joint due to the bending moment of the rod at the interface M_o due to the lateral deformation of the rod. The second is the resisting-moment component of the joint due to the axial forces perpendicular to the grain P_{ij}, i.e., axial forces of the steel rods and embedment of each member at the interface.

Contribution of the lateral deformation component

As the column-to-beam joints with GIRs must transmit the bending moment, the sectional forces in the rods must be in equilibrium at the interface between beam and column, as in Fig. 6. The bending moment in the rods at the interface must also be in equilibrium with the moment resulting from the lateral stress components σ_{ij} along the rod axis.

Thus, the bending moment of the *i*-th rod at the interface resulting from the lateral force component of the rods inserted in the beam (M_{oi}), when using the lateral force component of rod σ_{ij} and the distance from the interface between beam and column x_{ijs}, is expressed as:

$$M_{oi} = \int_0^{t_{ij}} \sigma_{ij} x_{ij} dx_{ij} = \int_0^{t_{ij}} k_{ij}\left(x_{ij}\right) v_{ij}\left(x_{ij}\right) x_{ij} dx_{ij} \tag{3}$$

where k_{ij} is the bearing constant of the *i*-th rod in the *i*-th member, and subscript j holds the value of 1 for column and 2 for beam.

Equation (3) differentiated twice, results in:

$$\frac{d^4 v_{ij}\left(x_{ij}\right)}{dx_{ij}^{\ 4}} + 4\lambda_{ij} v_{ij}\left(x_{ij}\right) = 0 \tag{4}$$

This gives the general solution:

$$v_{ij}(x_{ij}) = \Gamma_{ij}\sin\lambda_{ij}x_{ij} \cdot \cos\lambda_{ij}x + \Pi_{ij}\sin\mathrm{h}\lambda_{ij}x_{ij} \cdot \cos\lambda_{ij}x_{ij} + \Lambda_{ij}\sin\lambda_{ij}x_{ij} \cdot \cos\mathrm{h}\lambda_{ij}x_{ij} + \Xi_{ij}\sin\mathrm{h}\lambda_{ij}x_{ij} \cdot \cos\mathrm{h}\lambda_{ij}x_{ij}$$

where t_{ij} is the embedding length of the *i*-th rod, v_{ij} is the bearing displacement of *i*-th rod of the *j*-th member at x_{ij}, Γ_{ij}, Π_{ij}, Ξ_{ij}, and Λ_{ij} are undetermined coefficients, and

$$\lambda_{ij} = \sqrt[4]{\frac{k_{ij} d_i}{4(\mathrm{EI})_{si}}}$$

where $(\mathrm{EI})_{si}$ is the bending stiffness of the *i*-th rod, and d_i is the diameter of the *i*-th rod.

Equation 4 is well known as it is in agreement with the theory of a beam on an elastic foundation. It means that the elastic lateral stress components of the rod clearly depend on the lateral deformation of the rods.

The aim of this model was to derive the design method of rotational spring and strength for structural design. It is useful to divide the moment–rotation relationship from the shear–shear deformation relationship. For this reason, in

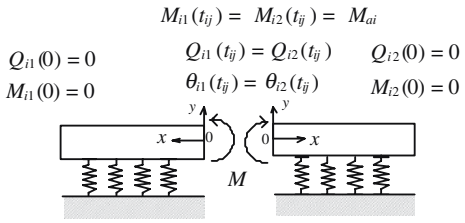

Fig. 7. Boundary conditions

the following model of stiffness, only the moment–rotation relationship is taken into account.

Figure 7 shows the boundary conditions for this model. At the interface between beam and column, the equilibrium condition of both bending moment and shear force, and the compatibility of the rotation angle were given. The bending moment was introduced at the interface as an action. The ends of the rods at a distance from the interface can be assumed as free ends, i.e., both shear force and bending moment were equal to zero. From above, the lateral displacement as a function of the distance from the interface, v_{i1} was derived as:

$$v_{i1} = \frac{-M}{2\lambda_{1i}{}^2 \mathrm{EI_s}} \cdot \frac{B(F-H-2D)\lambda_{2i}{}^2 + E(C-1)\lambda_{1i}\lambda_{2i} + A(G-C)\lambda_{1i}{}^2}{B(G-C)\lambda_{2i}{}^2 + A(C+H+2D)\lambda_{1i}{}^2} \tag{5}$$

where

$$A = \cos\lambda_{2i}t_{2i}\sin\lambda_{2i}t_{2i} - \cosh\lambda_{2i}t_{2i}\sinh\lambda_{2i}t_{2i},$$
$$B = \cos\lambda_{2i}t_{2i}\sin\lambda_{2i}t_{2i} + \cosh\lambda_{2i}t_{2i}\sinh\lambda_{2i}t_{2i},$$
$$C = \cosh^2\lambda_{1i}t_{1i} + \cos^2\lambda_{1i}t_{1i},$$
$$D = \cos\lambda_{1i}t_{1i}\sin\lambda_{1i}t_{1i}\cosh\lambda_{1i}t_{1i}\sinh\lambda_{1i}t_{1i},$$
$$E = \cosh^2\lambda_{2i}t_{2i} - \cos^2\lambda_{2i}t_{2i},$$
$$F = \cosh^2\lambda_{1i}t_{1i} + \cos^2\lambda_{1i}t_{1i},$$
$$G = \cosh^4\lambda_{1i}t_{1i} + \cos^4\lambda_{1i}t_{1i},$$
$$H = \cosh^4\lambda_{1i}t_{1i} - \cos^4\lambda_{1i}t_{1i}$$

Dependent on the left or right part of the v_{i2}, subscripts 1 and 2 should be exchanged.

In actual cases, as the complicated stresses work in steel rods, the model of Fig. 7, strictly speaking, does not hold good without axial deformations of rods. However, it can be considered that small effects due to the axial deformation of steel rods do, with miniscule axial deformation of rod, contribute to influencing factors like the deflection of the steel rods in the embedded parts and the bending moment of steel rods at the interface. The aim of this model is to derive the closed-form design equation as simply as possible. From this perspective, it was considered that modeling of the complicated stresses at work in steel rods more strictly would be of little value, because the resultant equations would be much more complicated. Thus, it was assumed that the model of Fig. 7 held good with miniscule axial deformation of rod.

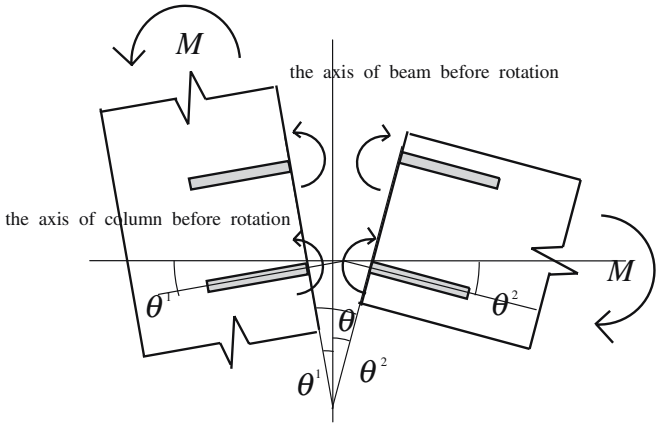

Fig. 8. Definition of rotational angle on glued-in rod (GIR)

The rotational angle of the moment-resisting joint was defined using v_i and t_i as follows (Fig. 8):

$$\theta = \theta_1 + \theta_2, \tag{6}$$

where

$$\theta_j = \frac{v_j}{t_j}$$

θ is the rotational angle of the joint, θ_1 is the rotational angle of the column, and θ_2 is the rotational angle of the beam.

The total moment M_o was defined as the sum of the moments caused by the lateral force component in each rod.

Therefore, the rotational stiffness R_{la} due to lateral force component of the rods was found to be:

$$R_{la} = \sum 2\lambda_{1i}{}^2 \mathrm{EI_s} \cdot \frac{B(G-C)\lambda_{2i}{}^2 + A(C+H+2D)\lambda_{1i}{}^2}{B(F-H-2D)\lambda_{2i}{}^2 + E(C-1)\lambda_{1i}\lambda_{2i} + A(G-C)\lambda_{1i}^2} \tag{7}$$

Contribution of the axial force component

For the moment caused by the axial force component M_a, the model of Komatsu et al.[5] was modified to this situation. Similar to the previous model,[5] strain at the i-th steel rod ε_{it} is expressed as:

$$\varepsilon_{it} = \frac{g_i - \lambda}{\rho}(i = 1,2) \tag{8}$$

where g_i is the distance from the compression of the outer surface to the center of the i-th steel rod line (i = 1,2), λ is the distance from the compression of the outer surface to the neutral axis (N-N), and ρ is the radius of curvature.

Putting E_{it} as an apparent modulus of elasticity along the i-th steel rod line, the stress corresponding to the strain ε_{it} is:

$$\sigma_{it} = E_{it} \cdot \varepsilon_{it} = E_{it}\frac{(g_i - \lambda)}{\rho}(i = 1,2) \tag{9}$$

In the model of Komatsu et al.,[5] only one member was considered using a symmetry condition; however, the situation considered in this case is nonsymmetrical. Thus, using the relative slip of GIR between beam and column, the whole joint was considered. E_{it} was substituted with a series system of an apparent modulus of elasticity along the *i*-th steel rod line of beam and column $E_{i\text{th}}$.

On the other hand, strain at the outermost surface of the compression side ε_c is:

$$\varepsilon_c = \frac{\lambda}{\rho} \tag{10}$$

Here, at the contact areas of both members, compression perpendicular to the grain of the column and compression parallel to the grain of the beam occur. Because the modulus of elasticity perpendicular to the grain is very small compared with that parallel to the grain, the compression perpendicular to the grain is dominant. Thus, in this model, compression parallel to the grain was assumed as rigid, and all embedment at the contact area was caused by compression perpendicular to the grain of the column.

Putting E_{90} as the modulus of elasticity perpendicular to the grain of the glulam member, the stress corresponding to the strain ε_c is:

$$\sigma_c = E_{90}\frac{\lambda}{\rho} \tag{11}$$

The resultant compression force due to embedment of each member *C* is:

$$C = b\int_0^{\lambda}\frac{y}{\lambda}\sigma_c dy = \frac{bE_{90}\lambda^2}{2\rho} \tag{12}$$

The resultant compression force *C*, which is to be sustained by the *i*-th rod line is:

$$C_i = \sigma_{it}\cdot A_{id}\cdot n_i = \frac{E_{i\text{th}}A_{id}n_i\left[\lambda-\left(h-g_i\right)\right]}{\rho} \tag{13}$$

The resultant tensile force T_i which is to be sustained by the *i*-th rod line is:

$$T_i = \sigma_{it}\cdot A_{id}\cdot n_i = \frac{E_{i\text{th}}A_{id}n_i\left(g_i-\lambda\right)}{\rho} \tag{14}$$

where A_{id} is the cross-sectional area of the steel rod belonging to the *i*-th line, *n* is the number of s belonging to the *i*-th steel rod line.

Similar to the deviation of the model of Komatsu et al.,[5] the rotational rigidity R_j due to the axial component could be derived as:

$$R_j = \sum_{i=1}^{2}\left(g_i-\frac{\lambda}{3}\right)\left(g_i-\lambda\right)n_iK_{si} \tag{15}$$

where

$$\lambda = -\beta_a + \sqrt{\beta_a^2+\mu_a}, \quad \beta_a = \frac{\sum K_{si}n_i}{bE_{90}},$$

$$\mu_a = \frac{2\sum K_{si}n_i\left(g_i-h\right)-2\sum K_{si}n_ig_i}{bE_{90}}, \text{ and}$$

$$K_{si} = \frac{K_{si1}K_{si2}}{K_{si1}+K_{si2}},$$

K_{si} is the relative axial slip modulus of glued-in steel rod between beam and column, K_{si1} is the axial slip modulus of glued-in steel rod in beam, K_{si2} is the axial slip modulus of glued-in steel rod in column, and λ is the neutral axis.

Combined bending moment due to axial and lateral deformation components

The moment capacity of the moment-resisting joint was defined as the sum of the moment due to axial and lateral components for the same rotational angle. Assuming superposition of both contributions is valid:

$$M = M_a + M_o \tag{16}$$

Strength of glued-in rod

Using Eq. 4, the shear force P_i of each rod at the interface introduced by the applied moment and applied shear force, on splitting failure due to glued-in rod, could be derived as:

$$P_i = \frac{-2\lambda_{2i}M}{\lambda_{1i}^{\ 2}}\cdot\frac{E\left(2D+H-F\right)\lambda_{1i}-BH\lambda_{2i}}{B\left(G-C\right)\lambda_{2i}^{\ 2}+A\left(2D-F-H\right)\lambda_{1i}^{\ 2}}+\frac{P}{n} \tag{17}$$

where *P* is the applied shearñ7orce, and *n* is the number of steel rods.

At the circle zones in Figure 9 (defined as the panel zone), the internal moment distribution is changed remarkably when compared with the exterior. This results in the shear stresses being concentrated. Therefore, the panel zone was taken as an area prone to shear failure.

$$M = \tau_{\text{wood}}th_1t_2 \tag{18}$$

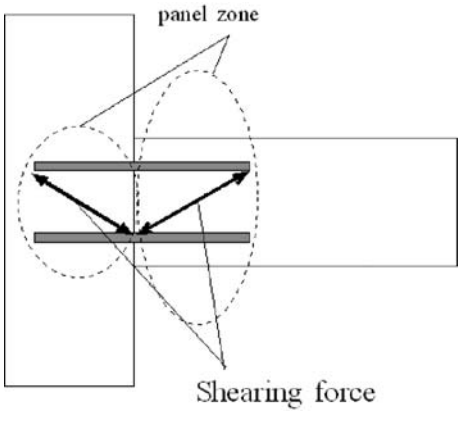

Fig. 9. Panel zones in GIR

where l_{1i} is the inserted length of the i-th rod.

In terms of the criteria of the axial shear stress component of rod, the model of Komatsu et al.[5] was modified.

$$M_{\max} = q_{1-\max}\left\{n_1\left(g_1 - \frac{\lambda}{3}\right) + n_2\left(g_2 - \frac{\lambda}{3}\right)\left(\frac{g_2 - \lambda}{g_1 - \lambda}\right)\right\} \quad (19)$$

$$M_{\max} = q_{2-\max}\left\{n_1\left(g_1 - \frac{\lambda}{3}\right)\left(\frac{g_1 - \lambda}{g_2 - \lambda}\right) + n_2\left(g_2 - \frac{\lambda}{3}\right)\right\} \quad (20)$$

where $q_{1\text{-max}}$ is the maximum pull-out strength of steel rod.

Theory proposal for the cross-lapped joint

Concept

Two main torsion theories exist: Coulomb's torsion theory and Saint Venant's torsion theory.[6] One may think that the torsion of glue lines can be explained using Coulomb's torsion theory, because the glue lines can be considered to be very thin. According to Goodier's hypothesis,[6] the torsion of arbitrary cross section with infinitely small length can be explained using Coulomb's torsion theory. However, because the modulus of elasticity and the rigidity of timber are not high when compared with those of the adhesive, the adhesive will force local deformation of the timber very close to the glue line. When the stress distribution in the glue line area is considered, it cannot be assumed that the effective widths of the glue lines are infinitely small.

Therefore, it is questionable whether the stress distribution at the glue line area can be explained using Coulomb's torsion theory. It was assumed that the effective width of the timber subjected to the torsion of glue line areas was not large enough to apply Saint Venant's torsion theory. Actually, it can be assumed that the stress distributions of most wooden glued joints have the characteristics of both theories.

The characteristic of Saint Venunt's torsion theory is that the stress at the shorter sides is much higher than that at the longer sides. Kelvin and Tait[7] found the necessary condition of this phenomenon. According to Kelvin (and demonstrated by Timoshenko and Goodier[6]), half the torque was due to the x-components of the shear stress and the other half to the y-components in Saint Venant's torsion theory. To extend Kelvin's hypothesis, a hypothesis was made that the moment due to x-components of shear forces is equal to that due to y-components.

$$M_{tx} = \frac{1}{2}M, \quad M_{ty} = \frac{1}{2}M \quad (21)$$

The characteristic of Coulomb's torsion theory (based on Goodier's hypothesis) is that the stress distribution is proportional to the rigid body displacement of the members. A hypothesis was made that the stresses in the glue line are initiated by the displacements of the members due to the bending and shearing deformation of timber. The theory for torsion was derived using these hypotheses.

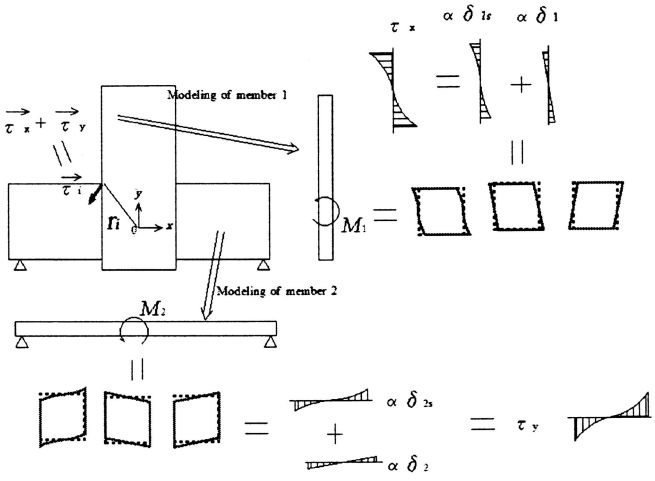

Fig. 10. Overview of mechanical model of cross-lapped joints (CLJs)

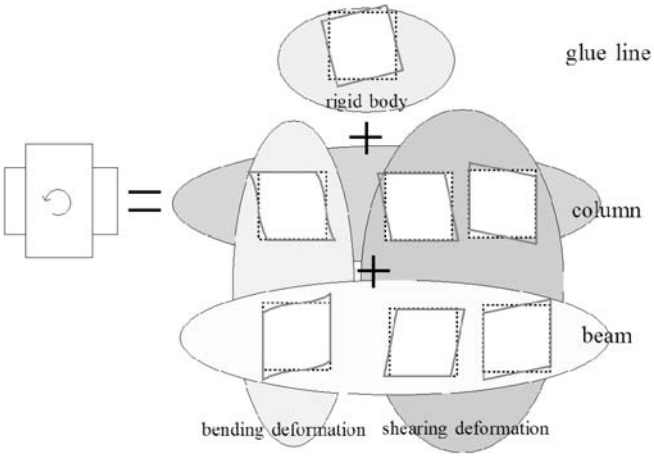

Fig. 11. Deforming components in CLJs

The parameters that play roles in the deformations were identified. An overview of the mechanical model for a CLJ is shown in Figs. 10 and 11, which show all possible deformations. It can be considered that the glue line areas are very thin and brittle, and do not contribute to joint rotation. The glue line areas were assumed to behave as rigid bodies, not because the glue lines are much more rigid than the timber, but because the glue lines are too thin and brittle to contribute to joint rotation.

Therefore, only the bending and shear deformation of timber were considered as the deforming components of the glued joint. The bending and shear deformation of each member at the panel zone was assessed using elementary beam theory.

Timber deformation

As the bending moment is transmitted from one member into another member at the panel zone, the bending moment of the panel zone changes along the length of the member. Shear force is also transmitted. To simplify the

analyses, the distribution of the shear stresses was assumed constant. First, the shear deformations of the panel zone δ_{js}, focusing on the timber member only, could be derived as follows:

$$\delta_{js} = \beta_a \frac{M_j}{G_j t_j b_j h_j} x_j \tag{22}$$

where, G_j is the shear modulus of the j-th member, t_j is the thickness of the j-th member, b_j is the height of the j-th member, h_j is the length of the panel zone of the j-th member, and β_a is an undetermined coefficient.

Timber bending deformations at the panel zone, using elementary beam theory, could be expressed:

$$Q_j(x_j) = \frac{M_j}{h_j} = \frac{d^3\delta_j}{dx_j^3} = \text{a constant} \tag{23}$$

Assuming that the deformation center of the panel zone, i.e., the rotation center for bending deformations and the shear center for shear deformations, corresponds to the geometrical center of the panel zone and does not deform. For this case, the following boundary conditions are valid:

$$M_j(0) = 0, \quad \delta_j(0) = 0, \quad \text{and } \theta_j(0) = 0 \tag{24}$$

With these boundary conditions and Eq. 23, the deflections of the beam due to bending moment $\delta_j(x_j)$ can be derived as follows:

$$\delta_j(x_j) = \beta_j \frac{M_j}{6h_j E_j I_j} x_j^3 \tag{25}$$

As illustrated in Fig. 10, superposition gives the total displacement as:

$$\delta_t = \left(\beta_a \frac{M_j}{G_j t_j b_j h_j} x_j + \beta_a \frac{M_2}{G_2 t_2 b_2 h_2} x_2 + \beta_j \frac{M_j}{6h_j E_j I_j} x_j^3 \right) \tag{26}$$

where β_j is an undetermined coefficient.

The next step is to determine the influence of the glue line deformation and how the shear stresses are distributed. Compatibility between the glue line and the timber member at the panel zone was considered. As mentioned earlier, the glue lines do not contribute to the deformation because it is assumed that it is infinitely stiff; therefore, the timber deformation in the panel zone close to the glue line area is restrained by the glue lines. Using this hypothesis, it is assumed that the shear stresses in the glue line τ_{jx} must be in equilibrium with the shear stresses in the timber and therefore relate to the deformation of the member. Following this reasoning and from Eq. 26, τ_{jx} can be expressed, introducing the new coefficient α, as follows:

$$\tau_{jx} = \alpha \left(\frac{M}{G_j t_j b_j h_j} x_j + \frac{M}{G_2 t_2 b_2 h_2} x_j + \frac{M_j}{6h_j E_j I_j} x_j^3 \right) \tag{27}$$

where α is an undetermined coefficient, which prevents timber deformation at the glue lines.

Because the resulting moment caused by the shear stresses must be equal to the sum of moments caused by all internal stresses, it follows:

$$M = \int\int \tau_{jx} x dx dy \tag{28}$$

Taking Eqs. 27 and 28, and eliminating α, τ_x, and τ_y, Eq. 29 can be obtained:

$$\begin{aligned} \tau_x &= \frac{30E_1I_1x + 5G_2t_2b_2^2x^3 + 5G_1t_1b_1^2x^3}{20E_2I_2b_2h_2^3 + 2G_2t_2b_2 2h_2^5 + 2G_1t_1b_1^2h_2^5} M, \\ \tau_y &= \frac{30E_2I_2y + 5G_2t_2b_2^2y^3 + 5G_1t_1b_1^2y^3}{20E_2I_2b_2h_2^3 + 2G_2t_2b_2 2h_2^5 + 2G_1t_1b_1^2h_2^5} M \end{aligned} \tag{29}$$

Rotational stiffness of cross-lapped joints

Estimation of rotational stiffness of cross-lapped joints was derived as follows. The apparent rotational deformation of a CLJ is the result of local deformation of each member at the panel zone. To estimate this effect, the energy method was used. The internal potential energy of the panel zone was expressed as total energy U at the joint:

$$U = \frac{1}{2}\int_0^h \frac{M^2}{EI} dx + \frac{1}{2}\int \frac{\gamma^2}{G} dx dy dz \tag{30}$$

Here, the influence of the glue lines must be considered in order to explain why the CLJs with five layers were more rigid than CLJs with three layers in the test results. It can, focusing on the timber member, be considered that the glue lines act to change the moment of the timber in the grain direction at the panel zone. Therefore, it was assumed that the direct effect of the glue lines was taken into account by considering the moment distribution along the panel zone length. However, there are certain differences between the members with a single-sided glue line and double-sided glue lines. It appeared as the effect of the thickness of the members. Assuming that the stress distribution along the width is constant, the average deformation along the width for double-sided glue line members is half as large as that with a single-sided glue line. This is related to the composition of the layers as shown in Fig. 12. The relative effect of the difference was taken into account afterward, introducing a thickness-direction-effect factor to divide the deformation of the member with two-sided glue lines by two single-sided glue lines.

Using the above and Castilian's first theorem, the rotational stiffness R is derived as follows:

$$R = \frac{1}{\sum_{\text{single-side-glueline}} \left(\frac{h_j}{G_j b_j t_j} + \frac{h_j^3}{6E_j I_j} \right) + \sum_{\text{two-side-glueline}} \left(\frac{h_j}{4G_j b_j t_j} + \frac{h_j^3}{24E_j I_j} \right)} \tag{31}$$

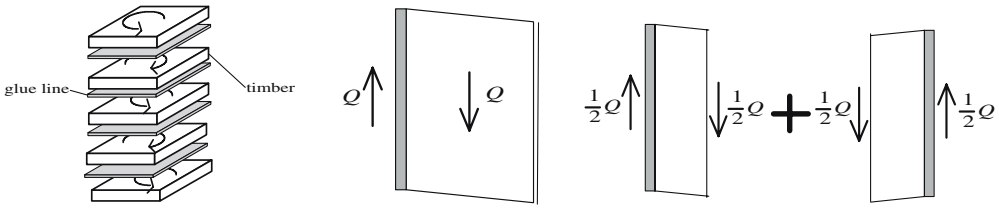

Fig. 12a–c. Concept of deformation of CLJ. **a** Panel zone, **b** single-sided glue line, **c** two-sided glue line

Strength of cross-lapped joints

The maximum shear stress of the glue line must appear at $x = h_1/2$ and $y = h_2/2$. Substituting $x = h_1/2$ and $y = h_2/2$ into Eq. 29, the shear stress component of the glue line can be expressed as:

$$\tau_x = \varphi M, \quad \tau_y = \psi M \tag{32}$$

where

$$\varphi = \frac{15E_1I_1h_1 + 0.625G_2t_2b_2^2h_1^3 + 0.625G_1t_1b_1^2h_1^3}{20E_2I_2b_2h_2^3 + 2G_2t_2b_2 2h_2^5 + 2G_1t_1b_1^2h_2^5},$$

$$\psi = \frac{15E_2I_2h_2 + 0.625G_2t_2b_2^2h_2^3 + 0.625G_1t_1b_1^2h_2^3}{20E_2I_2b_2h_2^3 + 2G_2t_2b_2 2h_2^5 + 2G_1t_1b_1^2h_2^5}$$

The resulting shear stress of the glue lines was calculated using Eq. 33.

$$\tau_i = \sqrt{\tau_{xi}^{\ 2} + \tau_{yi}^{\ 2}} = M\sqrt{\varphi^2 + \psi^2} \tag{33}$$

Assuming the glued joints (glue line) fail in brittle fashion, the maximum moment $M_{\max}$ is determined when somewhere near the shear strength is reached, i.e., τ_y. Therefore, $M_{\max}$ is expressed as:

$$M_y = \frac{\tau_y}{\sqrt{\varphi^2 + \psi^2}} \tag{34}$$

As another failure criterion, the shear failure of the timber at the panel zone was also taken into account (Fig. 13).

$$M = \tau_{\text{wood}} \sum t_i h_i b_i \tag{35}$$

where τ_{wood} is the shear strength of timber, t_i is the thickness of the i-th effective layer, h_i is the height of the i-th effective layer, and b_i is the length of the panel zone of the i-th effective layer.

Finally, for the case in which the joint is stronger than the members outside the panel zone area, the bending (and shear) failure of the members must be considered. However, it is known that for timber members of rectangular cross section, the shear strength is in most cases not governing factor and can therefore be ignored. In a CLJ, the effective thickness of each member at the interface is much smaller than that at nonpanel zones because at the panel zone some of the members are discontinuous. On the other hand, when the distances between the interfaces are very small, the strength cannot be predicted using the strength of the timber (timber with defects). In the case of very thin layers, the probability that the layer member at the interface has large defects compared with the defects along the beam is very small. For this reason, only the clear wood strength σ_{clear} for this particular zone was used. Using elementary beam theory, the equation for bending failure at the panel zone was derived as follows:

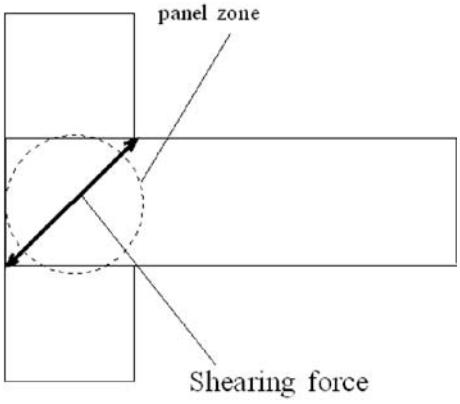

Fig. 13. Panel zone of CLJ

$$M_{\text{b}} = \sigma_{\text{clear}} Z_{\text{effective}} \tag{36}$$

where $Z_{\text{effective}}$ is the section modulus of effective layers.

Comparison between experiments and theory

The theory used in this study needs a number of basic material properties as input values. For that reason, the following parameters were determined for timber: E = 6.5 GPa, G = 430 MPa ($G = E/15$, $E_{90} = E/25$), and bearing constant k (embedment), in this case, was double the compression. Values calculated by Komatsu,[8] included the bending strength of clear wood 65 MPa (according to the old Japanese code), shear strength of glue line 4 MPa, and axial characteristics of GIRs: slip modulus of both inserted in parallel and perpendicular to the grain 50 kN/mm.[9] According to Eurocode 5,[10] the axial slip modulus of GIRs parallel and perpendicular to the grain are equal. The lateral strength of GIRs was calculated according to Blass et al.,[11] while the shear failure of the panel zone was based on Noguchi and Komatsu.[12]

Figure 14a, b compares the strength and stiffness values obtained by experiments with those from the proposed theory. As shown in Fig. 14, the initial stiffness and the

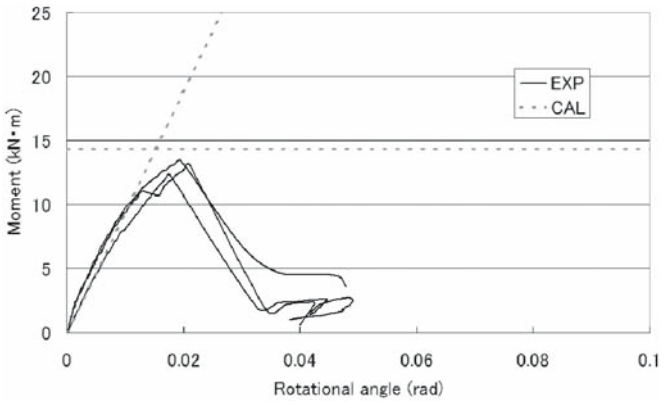

a

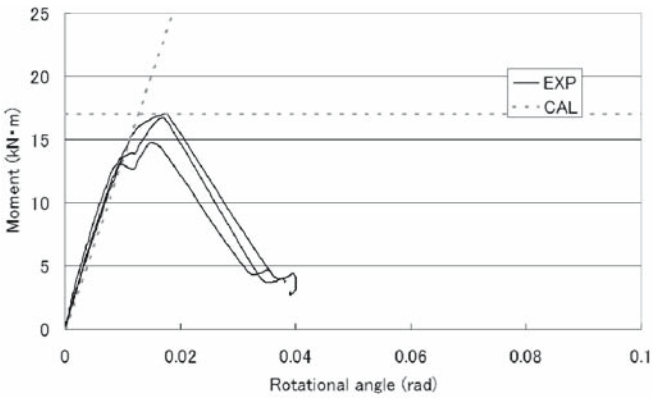

b

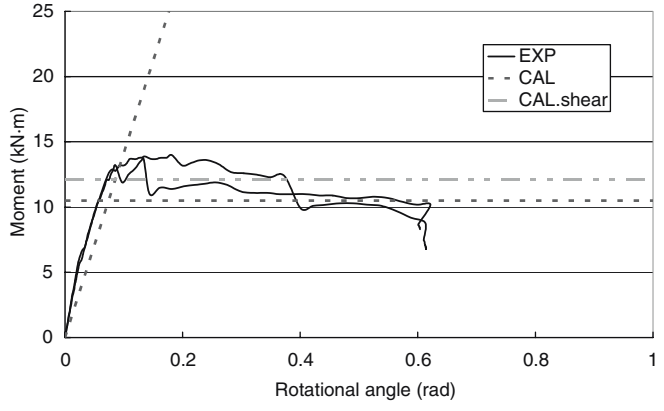

c

Fig. 14a–c. Comparison of experimental results and estimated values from the proposed theory. **a** Type A, **b** type C, **c** type E. *EXP*, experimental result; *CAL*, calculated values by proposed theory; *CAL.shear*, calculated strength by proposed theory considering only shear failure

strength in joint types A, C, and E were well predicted by the derived models. The strength criterion of CLJs (types A and C) was bending failure of the interface, as shown from experiment and theory. The strength of the joint with GIRs (type E) was limited either by splits occurring at the panel zone due to pulling out of the rod or by splitting failure caused by the lateral load component of the rods in the test. In Fig. 14c, the dashed horizontal line shows the value calculated using the criterion for the lateral force component of the rod, while the line of CAL shows that using the criterion for the pulling components of the rod. The calculation showed that the splitting criterion due to lateral force components in the rod was not governing, and that the shear force reached around 70% of the shear capacity. Indeed failure due to lateral force components in the rod actually occurred in the test. It was thought that the lateral component in the rod is a significant factor for stiffness and strength estimation of the GIR joint. The calculation shows that about 20% of the total stiffness could be accounted for by the lateral force component in the rod.

Conclusions

Design methods of moment-resisting joints using glued-in steel rods and cross-lapped glued joints are proposed. For CLJs, the hypothesis was made that both the rotational deformation and the glue line stresses develop due to the bending and shear deformation of the timber. In the GIR joints, not only the axial force components of the rod but also the lateral force component can be taken into account using the theory of a beam on an elastic foundation. Comparing the results predicted by the theory proposed with the experimental data for stiffness and strength of the CLJ and GIR joint, it was concluded that the predicting ability of the theory is very good. Based on the evaluation of the theory and experiments, it was concluded that the lateral force component in the rod is a significant factor in the stiffness and strength estimation of joints with GIR.

A moment-resisting joint stronger than the connecting timber members with the same cross section and stiff enough to be assumed rigid could be made using CLJs with three layers and GIRs. Therefore, it is thought that the members connected with this type of joint can be assumed as one solid member, disregarding the presence of a physical joint.

References

1. Komatsu K (1985) Strength design of cross-lapped glued joints for glulam portal frames (II): an approach to designing the strength of glued joints proving tensional stress is proportional to the distance from the rotation center. J Hokkaido For Prod Res Inst 402(1):1–9

2. Komatsu K (1985) Strength design of cross-lapped glued joints for glulam portal frames (I): an approach to designing the strength of glued joints proving glue lines suffer stress equivalent to those in a parallelogram bar subject to a pure tensional moment. J Hokkaido For Prod Res Inst 402(6):1–9
3. Komatsu K (1978) Strength of the joints with glued splint plates subjected to edgewise pure bending (in Japanese). Mokuzai Gakkaishi 49:19–86
4. Komatsu K (1984) Application of fracture mechanics to the strength of cross-lapped glued joints. FRI Bulletin 61, New Zealand Forest Service, New Zealand
5. Komatsu K, Koizumi A, Sasaki T, Jensen J, Iijima Y (1997) Flexural behaviour of GLT beams end-jointed by glued-in hardwood dowels. In: Proceedings of CIB W18-Timber Structures, Vancouver, CIB-W18/30-7-1
6. Timoshenko S, Goodier JN (1951) Torsion. In: Theory of elasticity. Kogakusha, Tokyo, pp 258–263
7. Kelvin WT, Tait PG (1912) Treatise on natural philosophy, vol 2. Cambridge University Press, pp 267–268
8. Komatsu K (1995) Moment resisting joint (in Japanese). In: Structural design note for timber structures. Maruzen, Tokyo, pp 184–221
9. Aicher S, Gustafsson PJ, Wolf M (2000) In: Proceedings of 1st RILEM Symposium on Timber Engineering, Stockholm, Sweden, pp 369–378
10. CEN/TC250/SC5 N158 (2001) Annex A: connections with glued-in steel rods. In: prEN 1995-1-1 Eurocode 5. CEN, Brussels, pp 105–108
11. Blass H, Görlacher R, Laskewitz B (2002) GIROD – glued in rods for timber structures. In: SMT4-CT97-2199, SP report, pp 34–43
12. Noguchi M, Komatsu K (2004) Design method of the knee sjoints using adhesive for the wooden portal frame structures. In: Proceedings of the WCTE, Lahich, vol 3, pp 301–304